COPLANAR STRIPLINE COMPONENTS FOR HIGH FREQUENCY APPLICATIONS

Kavita Goverdhanam**, Rainee N. Simons*, Nihad Dib**, Linda P.B. Katehi**
**Radiation Laboratory, University of Michigan, Ann Arbor, MI 48109-2122
*NASA Lewis Research Center, Cleveland, OH

Abstract

In this paper, coplanar stripline discontinuities such as a slit, a right angle bend and a T-junction are characterized and their performance is parameterized with respect to frequency and geometry. Lumped equivalent circuits are presented for some of them. The element values are obtained from the measured discontinuity scattering (S) parameters. The experimental results are compared with theoretical data obtained using the Finite Difference Time Domain (FD-TD) technique for validation and show very good agreement.

I Introduction

As with a coplanar waveguide (CPW), the coplanar stripline (CPS) [1] was introduced in the mid 70's as a transmission medium with the capability to provide uniplanar designs. However due to it's non balanced configuration, it has not found as wide applicability as the microstrip or the coplanar waveguide. CPS is used only in a handful of applications such as MMICs and feed networks for printed antennas [2], [3] and [4]. However, as the application moves to higher frequencies and the size of the substrate becomes critical in triggering parasitic modes and uncontrolled radiation, lines which show less dependence on wafer thickness become better candidates. Among these lines coplanar waveguide has attracted much more attention despite the limitations imposed by it's large ground planes and the excitation of parallel plate parasitic modes. The use of many vias to suppress these modes introduces many difficulties in design and fabrication resulting in poor performance and high cost. In view of the above disadvantages, coplanar lines with finite size grounds such as CPS require more attention. CPS has the capability to provide excellent propagation, when appropriately designed it has small discontinuity parasitics, it makes efficient use of the wafer area and can sustain back metalization without exciting parasitic modes within the range of the operating frequency. Lastly, heat sinking and packaging in high power applications (CPS power amplifiers) is simplified.

This work presents an extensive characterization of some important CPS discontinuities such as a CPS inductive slit, a right angle bend and a T-junction. The equivalent circuit model element values for these discontinuities are determined from the S parameters which are de-embedded from the measured S-parameters using a Thru-Reflect-Line (TRL) algorithm. The circuits are fabricated on a 762 μm thick RT-Duroid 6010 substrate ($\epsilon_r = 10.2$) having .5 oz copper cladding. The experimental results are compared to data obtained using the FD-TD method. The results which are presented for the very first time have potential applications in the emerging wireless communication and in the design of low cost uniplanar microwave circuits such as filters, mixers and antennas.

II Theoretical and Experimental Characterization

In a CPS [1], the electric lines from the strip conductors of width W extend across the slot of width S. The CPS is supported on a thin dielectric substrate of relative permittivity ϵ_r and thickness D as shown in Fig. 1. This work presents the study of a number of CPS discontinuities (see Figs. 2, 3 and 4), which find use in MMIC circuits. The study is performed theoretically as well as experimentally and the results are

0-7803-3246-6/96/$5.00 © IEEE

compared for validation purposes.

(a) Experimental Characterization : The measurements have been performed with the automatic network analyzer (HP8510C) using a TRL calibration technique. This technique utilizes on-wafer standards along with a pair of ground-signal RF probes. The standards consist of a CPS Thru, a CPS Short Circuit and a CPS Delay Line. The network analyzer is calibrated using National Institute of Standards and Technology (NIST) de-embedding software [5]. The reference impedance is set by the characteristic impedance Zo of the delay line.

(b) Theoretical Modeling : As mentioned above, the modeling was performed using the FD-TD method which is based on expressing Maxwell's curl equations in discretized space and time domains. In order to characterize any planar discontinuity, propagation of a specific time-dependent function is simulated using FD-TD technique. In characterizing the discontinuities mentioned above a Gaussian pulse was used. The space steps Δx, Δy and Δz, are carefully chosen such that integral numbers of them can approximate the dimensions of the structure. The Courant stability criterion is used to select the time step to ensure numerical stability. For the slit analyzed here the parameters used were $\Delta x = 110\ \mu m$, $\Delta y = 25\ \mu m$, $\Delta z = 36\ \mu m$, $\Delta t = .064$ ps and for the right angle bend the corresponding parameters were $110\ \mu m$, $35\ \mu m$, $35\ \mu m$ and.079 ps respectively. It is important to note at this point that the circuit dimensions indicated in the following figures are the actual dimensions after fabrication. However, while performing the FD-TD analysis the exact fabricated dimensions could not be incorporated due to limitations in the uniform discretization adopted in the modeling.

III Results and Discussion

In the following section, results for an inductive slit on a CPS line, a CPS right angle bend and a CPS T-junction (figures 2, 3 and 4 respectively) are presented. For all the discontinuities considered here the slot width is 101.6 μm and the strip width is 762 μm.

(a) Narrow slit in the CPS Strip Conductor: A narrow slit of width B and depth A in the CPS strip conductor is shown in Fig. 2. The slit is modeled as a lumped inductor L located between the planes P1 - P1' and P2 - P2' in series with the line. The inductance is determined from the discontinuity S-parameters of the circuit which are de-embedded from the measured S-parameters of the circuit. Figs. 5 and 6 show plots of the de-embedded and FD-TD modeled scattering parameters as a function of frequency for a slit of depth A = 531.9 μm and width of B = 180.3 μm. Fig. 7 shows the inductance as a function of the slit depth A. As expected, the inductance increases with the slit depth. It would be noteworthy at this point that for small values of the slit width the discontinuity can be modeled purely as an inductance to a very close degree of accuracy. However, if the slit depth is kept constant and the slit width B is varied, the discontinuity can no longer be modeled purely as an inductive element. For larger slit widths the discontinuity, which is now a CPS-step, needs to be modeled as an LC circuit where the capacitance, C becomes significant because the two sides of the slit (or step) are decoupled. Results to support this will be presented at the conference. Figures 5, 6 and 7 show a good agreement between the experimental and FD-TD results. The slight difference between the measured and FD-TD results can be attributed to the difference in dimensions between the fabricated structure and FD-TD model.

(b) CPS Right Angle Bend : A CPS right angle bend is shown in Fig. 3. The bend is modeled as a lumped T-network consisting of two series inductors L1 and a shunt capacitance C located between the planes O-P and O-P'. The equivalent T-network elements are determined from the de-embedded S-parameters of the circuit. As in the case of the CPS slit the results obtained from measurements are compared with the FD-TD modeled results. Fig.8 is a plot of the magnitude of the S-parameters obtained from measurement and FD-TD modeling as a function of frequency. The equivalent circuit element values for the bend will be presented at the conference. The reasons for the disagreements in the results are attributed to the use of 1st order absorbers at the edges of the FD-TD model instead of higher order absorbers.

(c) CPS T-junction: Fig. 4 shows a CPS in-phase T-junction. The measurements of the magnitude and phase of S31 as a function of frequency are shown in Figs. 9 and 10 respectively. The power coupled to the output ports 2 and 3 is the same in amplitude and phase and here only S13 is shown.

IV Conclusion

The coplanar stripline as a transmission medium holds a great deal of potential because of several advantages such as, excellent propagation, small discontinuity parasitics and efficient use of wafer area. In view of these advantages, modeling of some CPS discontinuities which have several technical and commercial applications was performed as a function of frequency and geometry. Good agreement was found between the experimental and theoretical results.

V Acknowledgments

The authors are greatful to the office of Naval Research
for funding the project and to Jong-Gwan Yook of the Univ. of Michigan for his patience in running the codes and have benefited from several discussions with him.

References

[1] J. B. Knorr and K. D. Kuchler, "Analysis of coupled Slots and Coplanar Strips on Dielectric Substrate", IEEE Trans. Microwave Theory Tech., Vol. MTT-23, No. 7, 541-548, July 1975. July 1975.

[2] M. Y. Frankel, J. F. Whitaker and G. A. Mourou, "Optoelectronic Transient characterization of Ultrafast Devices", IEEE Journal of Quantum Electronics, Vol. 28, No. 10, pp. 2313 - 2324, Oct. 1992.

[3] R. N. Simons, G. E. Ponchak, R. Q. Lee and N. S. Fernandez, "Coplanar Waveguide Fed Phased array Antenna", Digest of the 1990 IEEE Antennas and Propagat. International Symposium., Vol. 4, pp. 1778 - 1781.

[4] R. N. Simons, N. I. Dib, R. Q. Lee and L. P. B. Katehi, "Integrated Uniplanar transition for Linearly Tapered Slot Antenna", IEEE Trans. Antennas and Propagation, Vol. 43, No. 9, Sept. 1995.

[5] NIST De-embedding Software, Program DEEMBED, Revision 4.04, 1994.

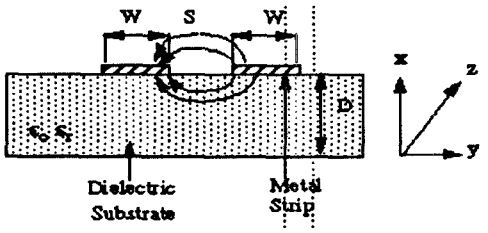

Figure 1: Cross Section of CPS

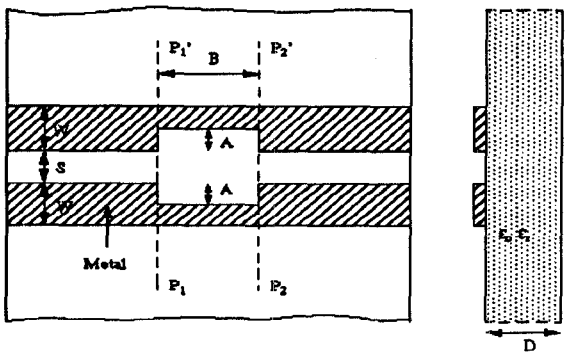

Figure 2: CPS Slit.

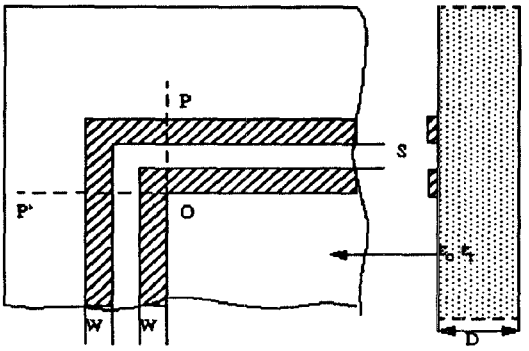

Figure 3: CPS Right Angle Bend.

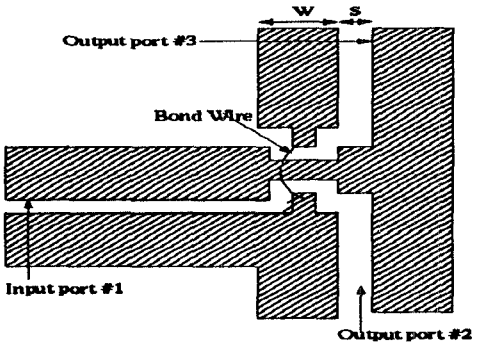

Figure 4: CPS T-junction.

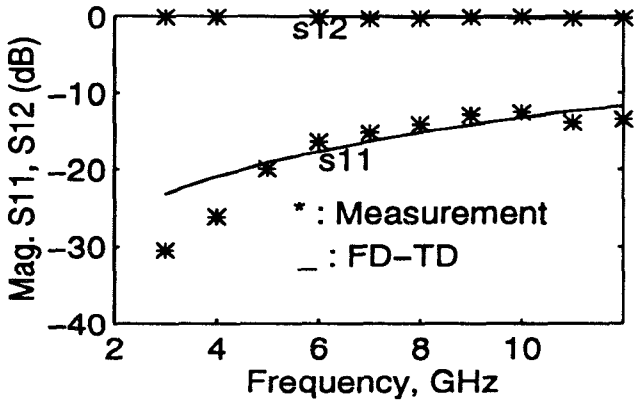

Figure 5: Magnitude of S11 and S12 for CPS slit; A = 531.9 μm, B = 180.3 μm.

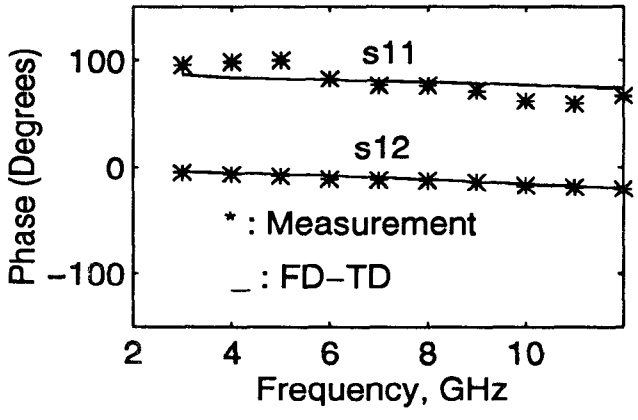

Figure 6: Phase of S11 and S12 for CPS slit; A = 531.9 μm, B = 180.3 μm.

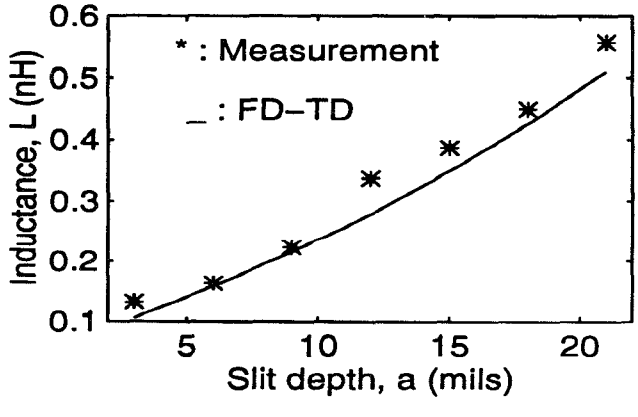

Figure 7: Inductance Vs Slit depth at 9GHz.

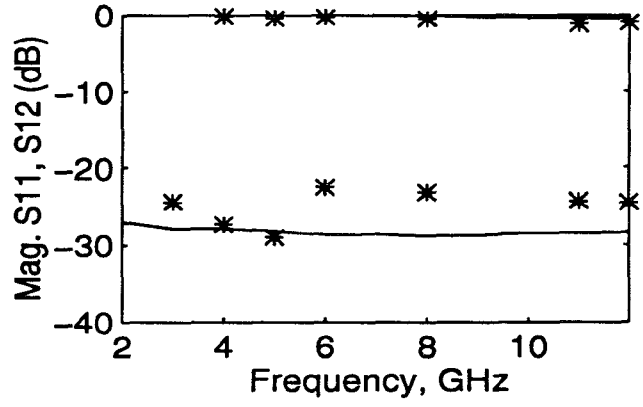

Figure 8: Magnitude of S11 and S12 for CPS bend; S = 101.6 μm.

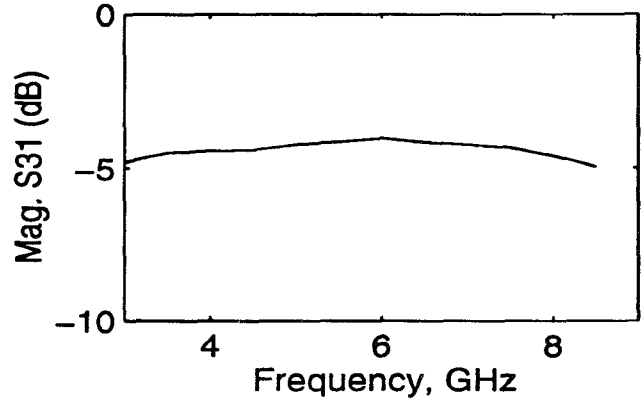

Figure 9: Measured magnitude of S31 for a CPS T-junction.

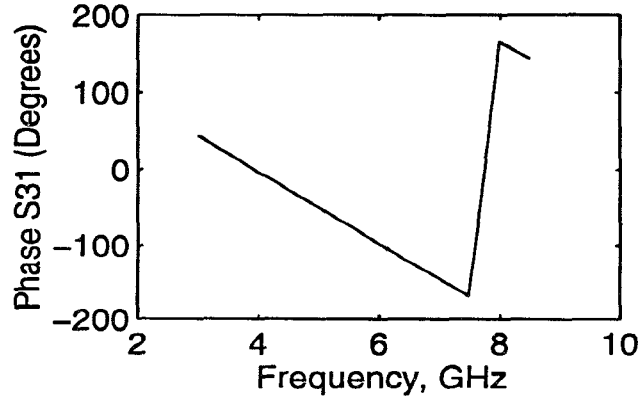

Figure 10: Measured phase of S31 for a CPS T-junction.